RESEARCH CONCERNING MATERIAL REMOVAL AT SINGLE PULSE LASER

Daniel Ghiculescu[1], Andrei Rusu[2], Cornel Enciu[3], Alexandra Barascu[4], Alina Chifelea[5], and Irina Grigore[6]

[1]National University of Science and Technology, "Politehnica", Bucharest *Corresponding author*, ORCID No. 0000-0001-6963-8350, daniel.ghiculescu@upb.ro
[2] National University of Science and Technology, "Politehnica", Bucharest ORCID No. 0009-0005-8922-0898, andrei.rusu@inflpr.ro
[3] National University of Science and Technology, "Politehnica", Bucharest ORCID No. 0000-0001-8905-4571, cornel.enciu@upb.ro
[4]National University of Science and Technology, "Politehnica", Bucharest ORCID No. 0009-0004-5205-2352, mariaalexandrabarascu@gmail.com
[5]National University of Science and Technology, "Politehnica", Bucharest ORCID No. 0009-0000-4510-1946, chifeleaalinastefania@gmail.com
[6]National University of Science and Technology, "Politehnica", Bucharest ORCID No. 0009-0001-8277-3407, irina.grigore2411@gmail.com

ABSTRACT: The paper deals with experimental research on single pulse laser of some useful material used in different industries as Al 1050, aluminum alloy anodized, stainless steel AISI 304, and Ti technical pure, grade 2. Some data concerning the state of art laser ablation, applicability, and working parameters are presented. The surfaces obtained by single pulse laser machining were studied by Scanning Electron Microscope (SEM), and correlations between experimental data and working parameters. Numerical simulations of the single pulse laser were approached for deeper understanding of the specific removal mechanism at different working parameters.

KEYWORDS: laser ablation, Al 1050, AISI 304, Ti, numerical simulation.

1. INTRODUCTION – STATE-OF-THE-ART

Laser ablation is characterized as small volume of material removal aimed at high accuracy, such as micromachining, and even nano level [1]. A plasma plume formed by different particles like photons, electrons, ions, atoms, molecules, liquid or solid particles is generated by a laser beam with low wavelength and very short pulse duration. Thus, an instant local vaporization on the surface of a target material is produced [2]. This is called *laser ablation* from *ablatio*, Latin word meaning "removal" or "taking off". In a broad sense, a small material removal could be considered an ablation, but at relative long pulses, the process moves from instant vaporization to thermal dominant process with heat dissipation in the volume of the machined workpiece, the case of the present research. A frequent industrial application is *drilling in hard materials* (metals or ceramics) to obtain small and deep holes, with reduced heat-affected zones. This kind of small surface is required in aerospace for turbine components or in electronics for semiconductor processing (e.g. gallium nitride) [3]. *Surface texturing* is a widely spread application often used at automative parts that modifies surface roughness to improve adhesion for coatings, paints, or bonds. A single pulse can be sufficient for light texturing on metals like aluminum or stainless steel, but also nonmetallic materials [4, 5]. *Nanoparticles and material synthesis* is another field of applications of laser ablation in chemical industries as advanced materials. This consists in creating various nature of nanoparticles (e.g., metals, oxides) or structures like carbon nanotubes. These are obtained by ablating materials sources as targets in liquids or gases [6]. *Contaminant removal* of rust, oxides, paints, or coatings from metals is another field of applications of laser ablation, which addresses industrial maintenance in sectors like oil and gas, shipbuilding, as well as heritage conservation (e.g., cleaning works of art). High-power single pulses are focused on target contaminants with an energy below the ablation thresholds of the base material [7]. Another major field of applications is *marking and identification* that produce permanent engraved information like QR codes, serial numbers, or logos on very different materials like metals, plastics, and organics. This is fundamental in quality assurance for traceability, applied in all industries from automotive to consumer goods. Single pulses are used for etching, rapid precise engraving, thus avoiding multiple passes when materials are very sensitive [8]. *Tissue ablation and surgery* are considered minimally invasive procedures. This is used in ophthalmology (e.g. for corneal reshaping), dentistry (drilling dip without heat damage), and oncology (tumor removal

or skin resurfacing). For such fine biologic material removal, single ultrashort pulses are used that allow precise, the so-called *non-thermal* tissue removal [9]. *Chemical analysis* is another reliable field in which laser ablation is used as a sampling tool in techniques like *Laser Induced Breakdown Spectroscopy* (LIBS). This serves as elemental composition determination in mining, geochemistry, or criminology. A single pulse creates plasma for rapid on-site analysis with minimal preparation [10]. *Thin Film Deposition* is an application achieved by pulsed laser deposition (PLD), which ablates material to form coatings for superconductors or optics, used in electronics and photonics industries [11]. Applications in environment suppose *remote spectroscopy for surface analysis* [12]. Other related ones to energy field consist in producing 2D materials like *black phosphorus*, *allotrope* form of pure phosphorus, used for batteries and sensors since it has just a few atoms thick, and have areas in the cm^2 range [13].

2. EXPERIMENTAL RESULTS

The materials machined in this study were: aluminum alloy, Al 1050 anodized is high corrosion resistant used for apparatus parts from chemical, food, electronics industries; it has 99.5% aluminum, and anodization achieves a layer of 30-50 μm, growing the *superficial toughness and electric isolation* [14, 15]; austenitic stainless steel, AISI 304 has also high *corrosion characteristics, mechanical resistance* characteristics, and *weldability*, thus being used in different industries like chemical, medical, pharmaceutical, automotive, aerospace, energetics etc. [16]; Technically pure Ti 99.5% (grade 2) has a minimum of 99% Ti and also contains elements such as Fe, C, and N; it combines excellent properties of *strength, ductility and corrosion resistance*, being widely used in industries such as aerospace, medical and marine [17].

The experiments took place at Center for Advanced LASER Technologies - CETAL, part of the National Institute for Laser, Plasma and Radiation Physics - INFLPR Măgurele, using the equipment; TRUMPF TruLaser Robot 5020 with 6 axes number, repetition accuracy: ± 0.1 mm, maximum workpiece load 30 kg, maxim workpiece dimensions: 1400, 1200, 800 mm [18]. This is used for a wide range of industrial applications such as drilling, cutting, welding, melting, controlled micro structuring thin layers deposition, complex materials ablation; a disk laser source Yb-YAg TRUMPF TruDisk 3001, with characteristics: wavelength 1030 nm, spot diameter with used optical system 0.8 mm; power range with continuous adjustment 80 - 3000 W [19]. For each material / sample, single laser pulses were applied with different duration (ti) and powers (P), adapted to its characteristics.

The laser spot diameter was *dspot*=0,8 mm. Finally, the machined zones were analyzed by Scanning Electron Microscopy (SEM), using QUANTA INSPECT F50 SEM, resolution 1 nm, from *Politehnica* Bucharest.

The samples data corresponding to single pulse laser machining were synthesized in Table 1.

Table 1. Samples data for single pulse laser machining

Sample 1	Dimensions	Al 1050 anodized
	h [mm]	0,5
	l [mm]	42
	L [mm]	25
	Ra [μm]	6,3
Sample 2	Dimensions	AISI 304
	h [mm]	0,5
	l [mm]	80
	L [mm]	44
	Ra [μm]	0,4
Sample 3	Dimensions	Ti, grade 2
	h [mm]	9
	l [mm]	48
	L [mm]	20
	Ra [μm]	4,5

The disposal of the holes obtained by single pulse laser on the three samples, corresponding to the values of pulse time, is presented in figure 1.

Sample 1, Al 1050 anodized

Sample 2, stainless steel AISI 304

Sample 3, Ti, grade 2

Figure 1. Images of the samples after single pulse laser machining

Table 2. Microgeometry experimental

Sample	Shapes \ Pulse time	ti=5 ms	ti=10 n
1, Al1050 anodized	Microcracks	-	-
	Microcavities	11.33-58.64	34.36-65.98
2, stainless steel, AISI 304	Microcavities	0.81-5.98	10.58
	Borders	not noticed	40.56 116.5
3, Ti technically pure, grade 2	Microcracks	-	0.31
	Microcavities	339.8 948.8 955.9	1.13 0.82 19.89
	Borders	not noticed	265.8

Table 3. SEM images of microgeom

Material	Al 1050 anodized	Steel AI
Holes diameters	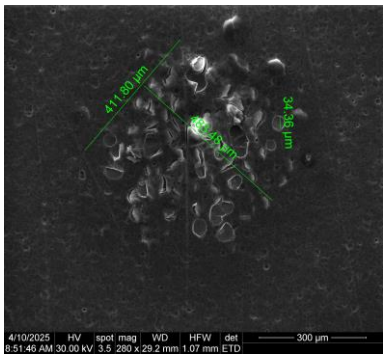	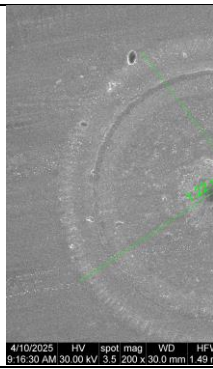
	P =300 W, ti = 5 ms	P = 600 W,
Micro-cracks	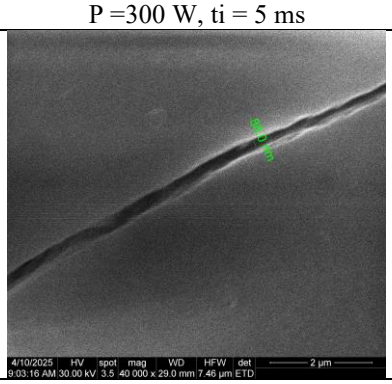	not not
	P = 300 W, ti = 15 ms	-
Micro-cavities	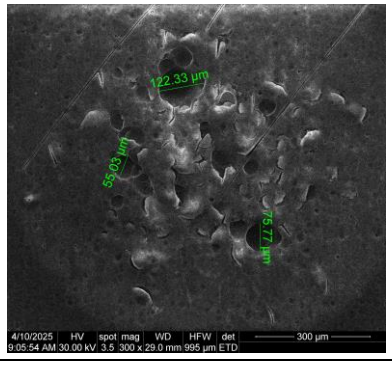	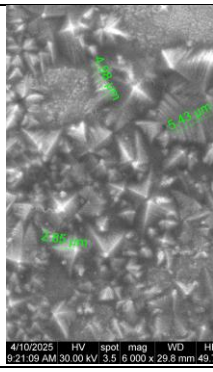
	P = 300 W, ti= 20 ms	P = 600 W,

Borders	not noticed	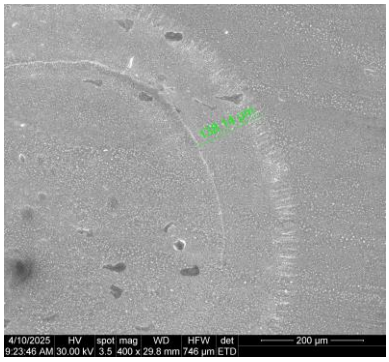	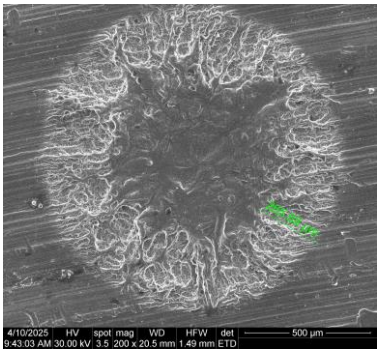
	-	P = 600 W, ti = 20 ms	P = 600 W, ti = 10 ms

Figure 2. Model parametrization for anodized Al 1050

The shapes and dimensions of the microgeometry, visualized at SEM, on the surfaces machined by single pulse laser at different values of pulse durations (*ti*) are presented in Table 2.

The images of details provided by QUANTA INSPECT F50 SEM of machined surfaces are presented in Table 3. As one can observe several types of shapes are identified on SEM images like microcracks, microcavities, borders as well as holes not pierced and pierced (at 0,5 mm thickness) with different values of diameters. Each of them was associated with values of working parameters, respectively laser power (*P*), and pulse durations (*ti*).

3. NUMERICAL SIMULATION OF SINGLE LASER PULSE MACHINING

The models for numerical simulations of single pulse laser machining were elaborated corresponding to each type of sample / category of material, using COMSOL Multiphysics, 2D dimensional space, Heat Transfer in Solids, Time dependent regime. The modeling comprises the following stages:

A. Parameterization of the models. The necessary parameters used in case of Al 1050, anodized (Al2O3, superficial layer) are described in figure 2:

Name	Expression	Value	Description
dspot	0.8[mm]	8E-4 m	laser spot diameter
gp	0.5[mm]	5E-4 m	sample thickness
l1	25[mm]	0.025 m	sample width
l2	42[mm]	0.042 m	sample length
rgaz	2.5[mm]	0.0025 m	radius of gas spot
Ttop	660+273.15	933.15	Al melting temperature
P	300[W]	300 W	laser power
sigma	dspot/6	1.3333E-4 m	standard deviation
A1	0.85	0.85	Al2O3 absorption coefficient
emi	0.2	0.2	Al2O3 emissivity coefficient
h1	10[W/(m^2*K)]	10 W/(m²·K)	ambient heat transfer coefficient
Ed	P/(pi*0.25*dspot^2)	5.9683E8 W/m²	power density on laser spot
ti	25[ms]	0.025 s	pulse time
gpan	30[um]	3E-5 m	thickness of anodized layer
Ttopan	2072+273.15	2345.2	anodized layer melting temperature
Ra	6.3[um]	6.3E-6 m	roughness Ra
Rsm	200[um]	2E-4 m	distance between microgeometry peaks
Rz	4*Ra	2.52E-5 m	roughness Rz
h2	100[W/(m^2*K)]	100 W/(m²·K)	gas heat transfer coefficient
xr	0	0	laser spot center

The parameters used at stainless steel AISI 304 machining are presented in figure 3.

Name	Expression	Value	Description
dspot	0.8[mm]	8E-4 m	laser spot diameter
gp	0.5[mm]	5E-4 m	sample thickness
l1	44[mm]	0.044 m	sample width
l2	80[mm]	0.08 m	sample length
rgaz	2.5[mm]	0.0025 m	radius of gas spot
Ttop	1450+273.15	1723.2	tmelting temperature of AISI 304
P	600[W]	600 W	laser power
sigma	dspot/6	1.3333E-4 m	standard deviation
A1	0.43	0.43	absorption coefficient of AISI 304
emi	0.7	0.7	emissivity coefficient of AISI 304
h1	10[W/(m^2*K)]	10 W/(m²·K)	ambient heat transfer coefficient
Ed	P/(pi*0.25*dspot^2)	1.1937E9 W/m²	power density on laser spot
ti	25[ms]	0.025 s	pulse time
Ra	0.4[um]	4E-7 m	roughness Ra
Rsm	200[um]	2E-4 m	distance between microgeometry peaks
Rz	4*Ra	1.6E-6 m	roughness Rz
h2	100[W/(m^2*K)]	100 W/(m²·K)	gas heat transfer coefficient
xr	0	0	laser spot center

Figure 3. Model parametrization for AISI 304 stainless steel

The parametrization used for numerical simulation of Ti grade 2 machining is presented in figure 4.

Name	Expression	Value	Description
dspot	0.8[mm]	8E-4 m	laser spot diameter
gp	9[mm]	0.009 m	sample thickness
l1	20[mm]	0.02 m	sample width
l2	48[mm]	0.048 m	sample length
rgaz	2.5[mm]	0.0025 m	radius of gas spot
Ttop	1688+273.15	1961.2	melting temperature of Ti [K]
P	600[W]	600 W	laser power
sigma	dspot/6	1.3333E-4 m	standard deviation
A1	0.85	0.85	absorption coefficient of Ti
emi	0.4	0.4	emissivity coefficient of Ti
h1	30[W/(m^2*K)]	30 W/(m²·K)	ambient heat transfer coefficient
Ed	P/(pi*0.25*dspot^2)	1.1937E9 W/m²	power density on laser spot
ti	25[ms]	0.025 s	pulse time
xr	0	0	laser spot center
Ra	4.5[um]	4.5E-6 m	roughness Ra
Rsm	200[um]	2E-4 m	distance between microgeometry peaks
Rz	4*Ra	1.8E-5 m	roughness Rz
h2	100[W/(m^2*K)]	100 W/(m²·K)	gas heat transfer coefficient

Figure 4. Model parametrization for Ti grade 2

B. Variables definition for energy distribution on laser spot was done by Gauss distribution function (*G_space*), taking account of absorption coefficients (A1) for each material of the samples, figure 5. This depends on the laser wavelength (λ=1030 nm) and the

surface state (oxidation, Ra). Finally, the Laser Heat Source (*LHS*) parameter resulted.

Name	Expression	Unit
G_space	exp(-(x-xr)^2/(2*sigma^2))	
Plaser	A1*Ed	W/m²
LHS	Plaser*G_space	W/m²

Figure 5. Variables definition on laser spot

C. Models geometry was created with Comsol built-in tools, using parameters from above. An example is presented in figure 6, for machining Al 1050, anodized (Al_2O_3, superficial layer).

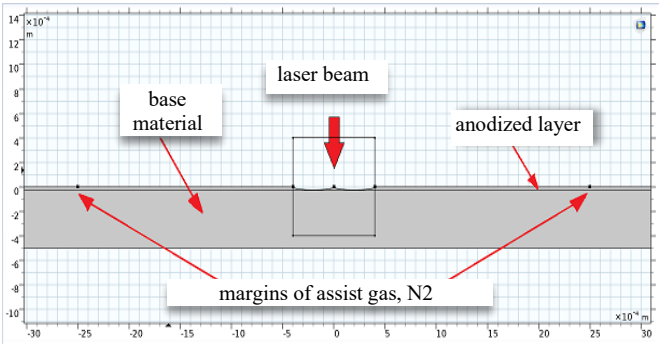

Figure 6. Geometry of the models

The laser spot is bordered by the frame formed using *dspot* width and covers 6 *sigma*.

D. Material properties for the three samples are introduced in figure 7:

Property	Variable	Value	Unit
Thermal conductivity	k_iso ; k...	30	W/(m·K)
Heat capacity at constant pressure	Cp	900	J/(kg·K)
Density	rho	3970	kg/m³

Anodized layer on Al1050

Property	Variable	Value	Unit
Thermal conductivity	k_iso ;...	16.2	W/(m·K)
Density	rho	8000	kg/m³
Heat capacity at constant pressure	Cp	500	J/(kg·K)

Stainless steel AISI 304

Property	Variable	Value	Unit
Thermal conductivity	k_iso ;...	20	W/(m·K)
Heat capacity at constant pressure	Cp	0.52[J/(g*K)]	J/(kg·K)
Density	rho	4510	kg/m³

Ti 99,5%

Figure 7. Material properties for the three samples

D. Mesh characteristics are presented in figure 8, with free triangular elements, and extremely fine size.

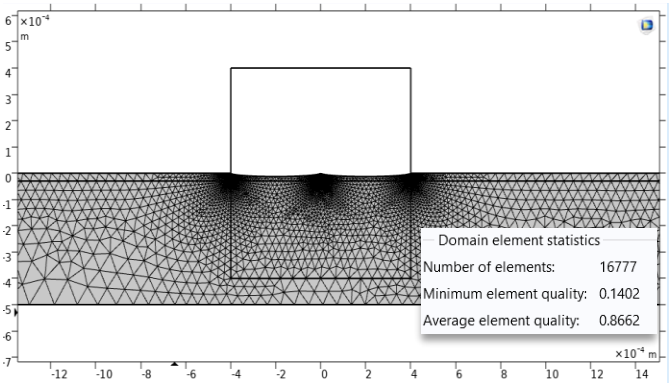

Figure 8. Mesh for sample Al 1050, anodized

One can notice that the models are not low size, so 2D is a rational option, avoiding large calculation resources.

E. Boundary conditions address the following: laser heat source (figure 9.a), forced convective cooling produced by assisting gas with coefficient *h2* (figure 9.b), convective cooling in environment heat transfer coefficient *h1* (figure 9.c), and radiant cooling in environment with coefficient *emi* (figure 9.d).

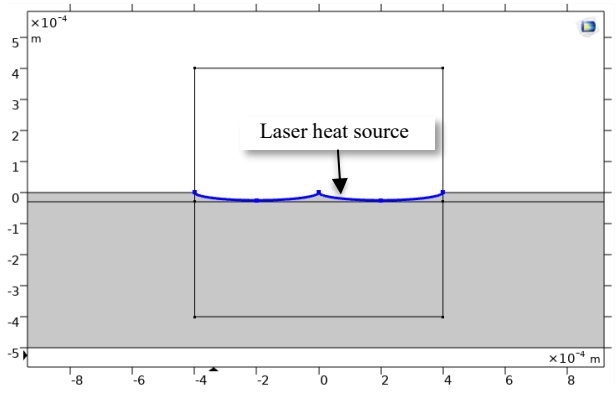

a) Laser Heat Source (LHS) – Heat flux

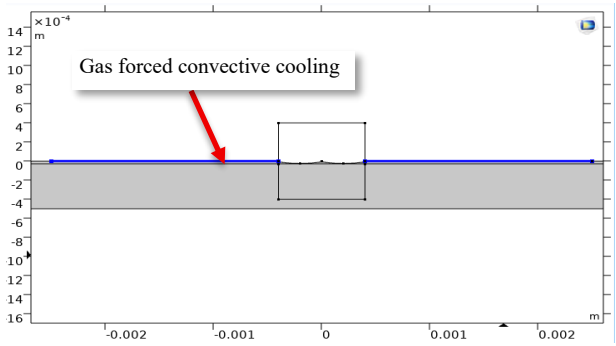

b) Forced convective cooling (h2)

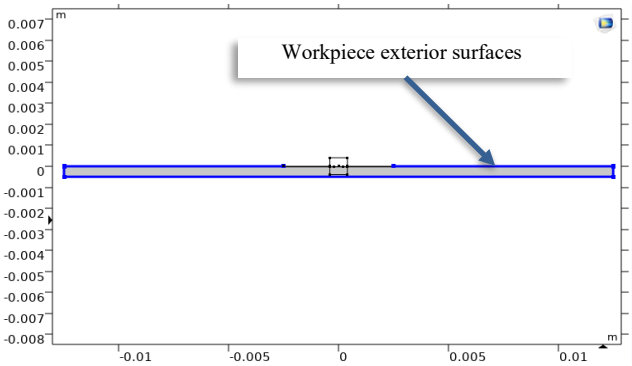

c) Convective cooling (h1)

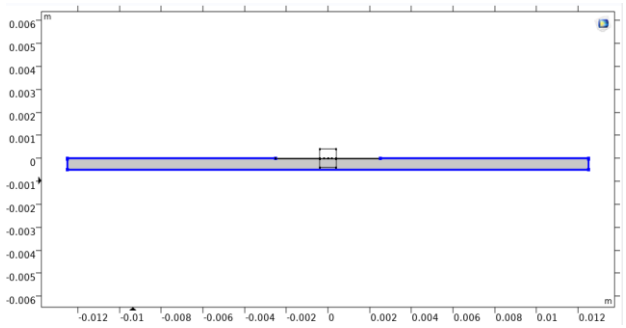

d) radiant cooling (*emi*)

Figure 9. Boundary conditions at single pulse laser machining

F. Simulation of single laser pulse machining was set as time dependent, using pulse time *ti*, and a step of 0.1**ti*, (figure 10).

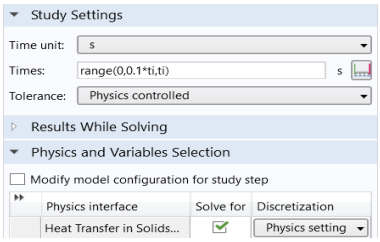

Figure 10. Time dependent study settings

4. SIMULATION RESULTS AND DISCUSSION

The results obtained from the numerical simulation contribute to deeper understanding of the complex phenomenology characterizing the single pulse laser machining.

In case of the Al 1050 sample machining, with an anodized surface layer approximately 30 µm thick, a complex material removal mechanism is revealed. This involved both a thermal and a mechanical component, the latter resulting from the significant temperature gradient induced by the laser pulse. Thus, in the first stage, the anodized layer, which has a much higher thermal resistance than the Al 1050 substrate, is removed.

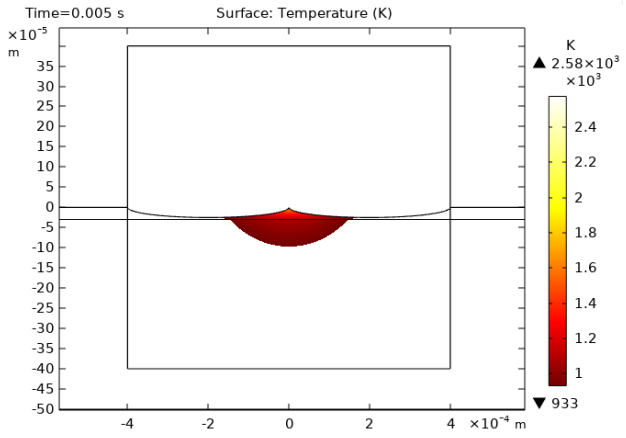

(a) Stage 1, pulse time ti=5 ms

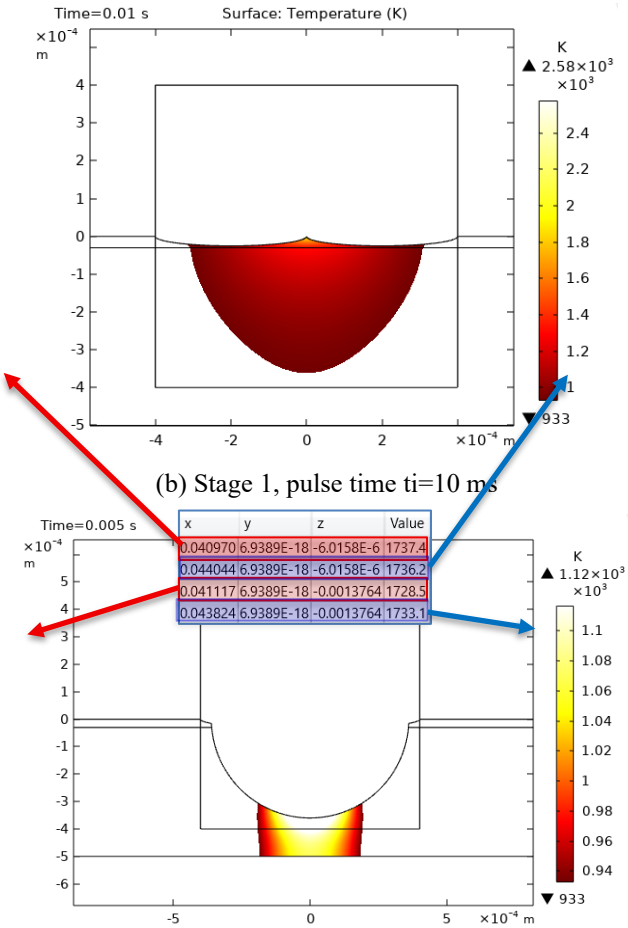

(b) Stage 1, pulse time ti=10 ms

(c) Stage 2, pulse time ti=15 ms (10+5 ms)

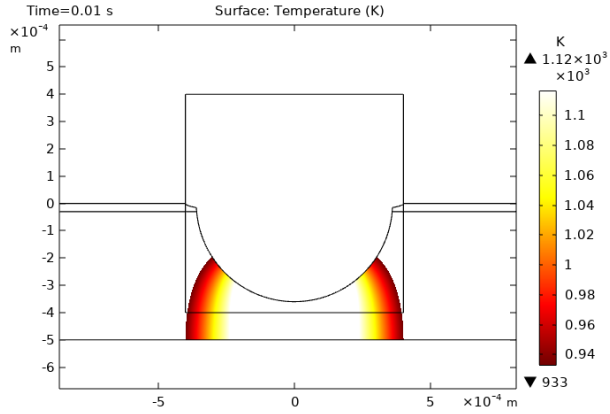

(d) Stage 2, pulse time ti=20 ms (10+10 ms)

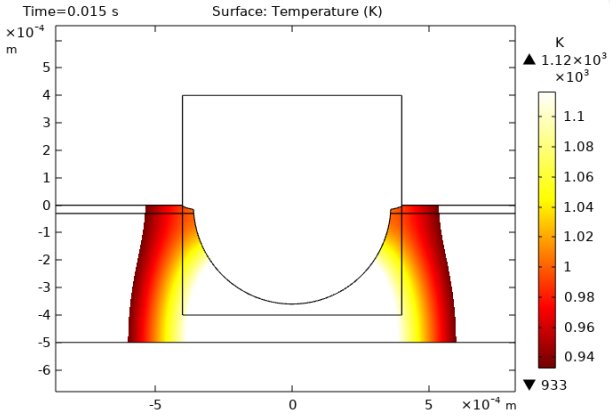

(e) Stage 2, pulse time ti=25 ms (10+15 ms)

Figure 11. The volume of removed material at the sample of Al 1050 anodized at laser single pulse, power, P=300 W

Although the melting temperature of aluminum oxide, 2072°C, is higher than that achieved at the laser spot in certain machining regimes (laser pulse durations), it could be removed through the vaporization of the Al substrate. This is due to its melting temperature of only 600°C, and the result is the formation of microcracks observed at SEM, with dimensions of 0.3-1.1 µm, and microholes with diameters of 11 - 122 µm (see Tables 2 and 3). After the removal of the anodized aluminum oxide layer, almost achieved after approximately 10 ms (Fig. 11, (a-b), the laser radiation directly removes the aluminum substrate in stage 2 (Fig. 11, (c-e). The volume of material on pulse is decreased in interval of 15–20 ms, determined by two factors:

(1) *the substrate absorption coefficient* that drops to A1=0.75 from the previous value of A1=0.85 of the surface layer; (2) *the higher thermal conductivity of aluminum*, approximately k=200 W/mK, compared to that of the surface layer, approximately k=10 W/mK; however, finally the *lower Al melting temperature* helps the penetration of the material.

The results obtained from the numerical simulation of the ablation process for AISI 304 stainless steel are presented in fig. 12. For increasing durations of a single laser pulse, while maintaining a constant power of P=600 W, which is higher than in the case of the previous material, an expected increase in the volume of material removed is observed as the pulse energy increases.

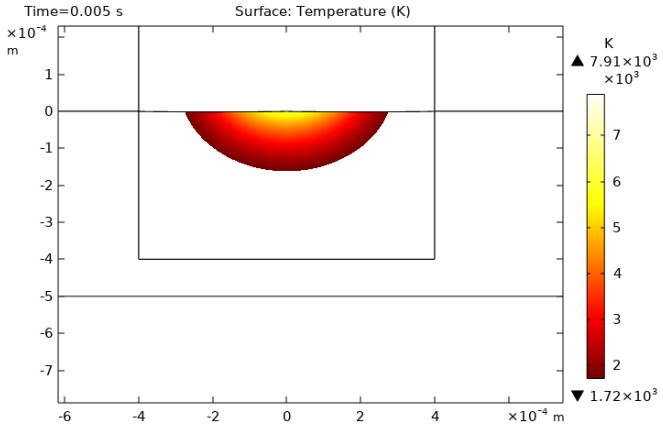

a) pulse time, ti=5 ms

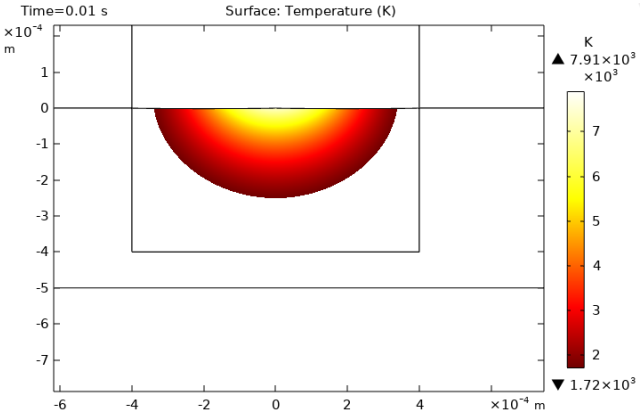

b) pulse time, ti=10 ms

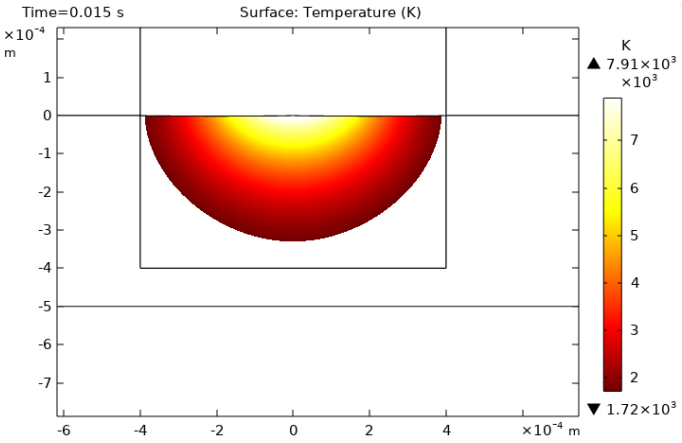

c) pulse time, ti=15 ms

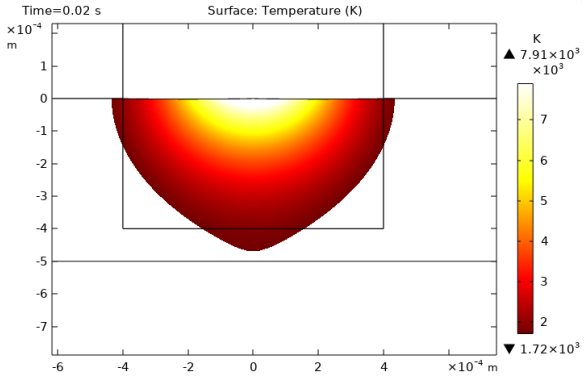

d) pulse time, ti=20 ms

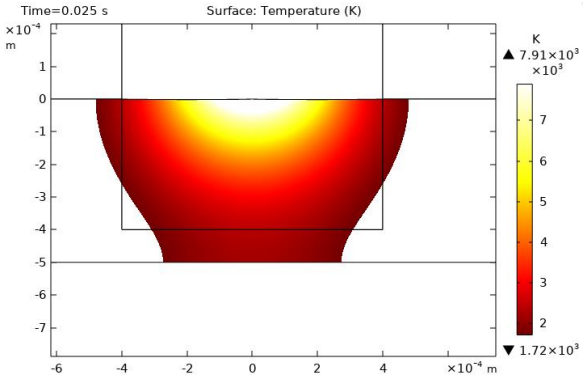

e) pulse time, ti=25 ms

Figure 12. The volume of removed material at the sample of AISI 304 at laser single pulse with power, P=600 W

The dimensions of the hole diameters obtained are consistent with experimental data, being larger than those for anodized Al 1050.

The behavior of AISI 304 stainless steel under the thermal shock induced by the laser pulse is superior to that of the previous material, as evidenced by SEM images, which show no microcracks. This steel has high ductility and responds well to internal tension caused by high thermal gradient. However, a circular crown (rim) with a thickness of 10–60 µm, exhibiting a distinct appearance, was observed on the outer surface of the hole, corresponding to the inflection point of the Gaussian curve, beyond which the energy distribution of the laser pulse decreases asymptotically along the x-axis.

The surface of the ablated hole exhibits microcavities identified via SEM, with transverse dimensions ranging from 0.9 to 100 µm, which increase with the laser pulse energy. This phenomena was also reported recently at laser machining AISI 304 [20, 21, 22].

This could be explained by the melting of the material under the action of a single laser pulse, where the recoil pressure, combined with capillary forces (surface tension) and thermocapillary forces (Marangoni effect, driven by the temperature gradient and active elements such as O or S), redistributes the molten material. The phenomenon arises from the surface tension, which is higher at the periphery, pulling the material outward and allowing the formation of gaseous microcavities within the molten pool [23]. In this case, the relatively long pulse duration (5–25 ms) creates a stable molten pool, where the Marangoni effect has sufficient time to influence fluid dynamics (unlike ultrashort fs/ns pulses, where thermal effects are minimal and characteristic of pure ablation). At the end of the pulse duration, rapid cooling of the molten zone occurs, preserving this microgeometry, with the microcavities inside as observed via SEM.

For the third ablated material, technically pure 99.5% Ti (Grade 2), the temperature distributions are presented in Fig. 13.

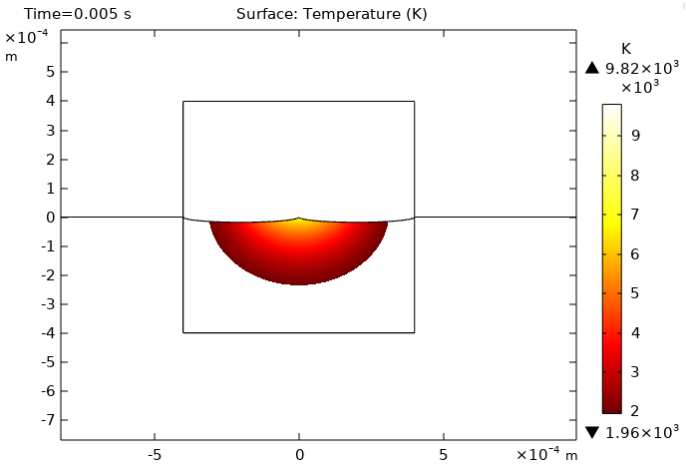

a) pulse time, ti=5 ms

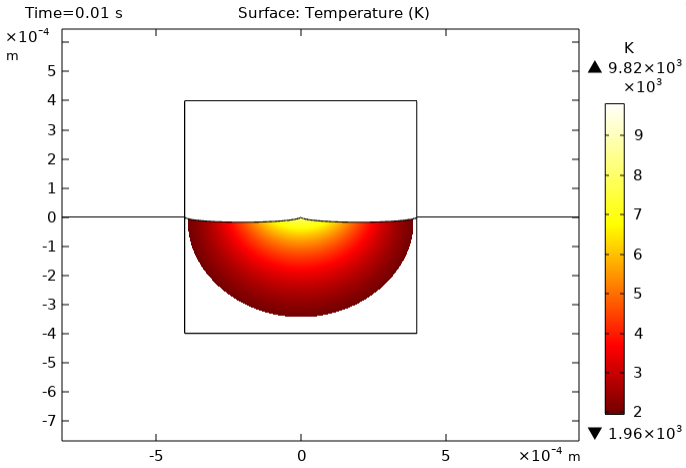

b) pulse time, ti=10 ms

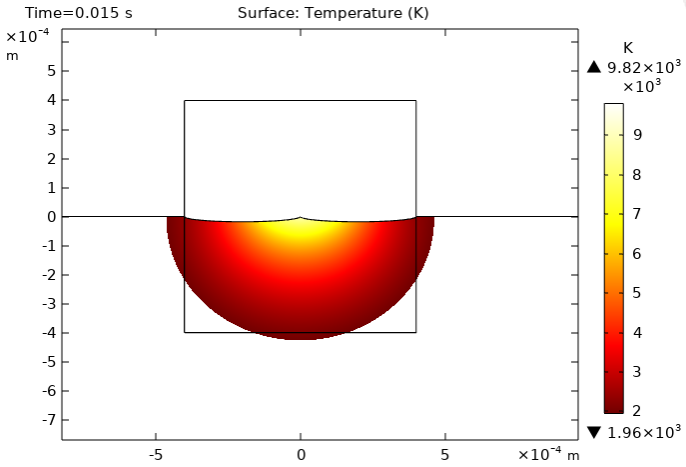

c) pulse time, ti=15 ms

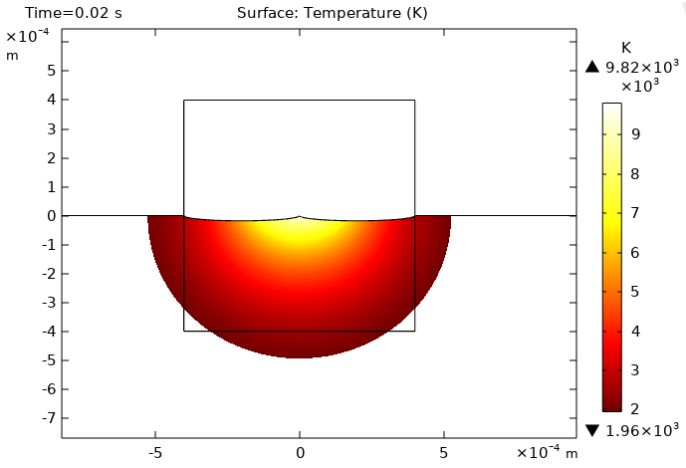

d) pulse time, ti=20 ms

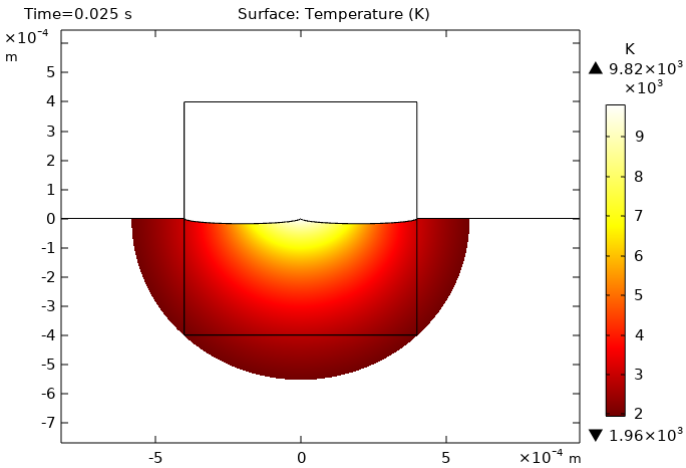

e) pulse time, ti=25 ms

Figure 13. The volume of removed material at the sample of Ti, grade 2, at laser single pulse with power, P=600 W

For this sample as well, SEM images revealed the presence of microcracks on the processed surface, with widths ranging from 0.3 to 0.85 μm.

This can be explained by two key parameters: thermal gradient and residual stress. Upon analyzing the thermophysical properties of the material, two factors stand out:

(1) *Higher thermal conductivity*: Ti exhibits a thermal conductivity of approximately 20 W/m·K, compared to about 16.2 W/m·K for AISI 304, where no such microcracks were observed. Consequently, the thermal energy induced by single pulse laser in the material dissipates more rapidly toward the interior, creating a significant surface gradient. After the laser pulse ends, during cooling, the material contraction is much stronger than in AISI 304, generating compressive stresses on the surface that propagate radial or reticular microcracks, as seen in the image presented in Table 3 (e.g., the 849 nm fissure).

(2) *Lower thermal expansion coefficient*: Ti has an α of ~8.6 × 10^{-6}/K, only half that of AISI 304, which has an α of ~17 × 10^{-6}/K. At first glance, this might seem advantageous, but in reality, during rapid cooling, the difference in expansion between zones - cold in the interior versus hot on the surface – it becomes more pronounced, leading to microcracks. In contrast, the higher thermal expansion of AISI 304 allows for plastic deformation, absorbing the stress and preventing the formation of microcracks.

Another explanation could be based on the difference in *crystalline structure and ductility* between the two materials [24].

Thus, Ti Grade 2 possesses a hexagonal close-packed (HCP) structure with fewer slip planes (only 3 independent directions), rendering it more fragile under rapid thermal deformations. Upon cooling, a phase transformation can occur, forming martensitic α' (tetragonally distorted), which is hard but brittle, thereby promoting microfissures (see Table 3).

In contrast, stainless steel AISI 304 has an austenitic structure (face-centered cubic, FCC), highly ductile, with 12 slip planes - allowing it to absorb shock through plastic deformation, resulting in only microcavities (e.g., gas bubbles trapped in the structure) rather than microcracks. This explains why AISI 304 displays better resistance to the thermal shock induced by the laser pulse.

A spongy structure is observed in the image from Table 3, which can be attributed to the rapid reaction of Ti with O_2 from the air at high temperatures, forming a *porous TiO_2 layer* - approximately 5–10 μm thick on the surface - which is fragile and facilitates the formation of microcracks. Furthermore, if traces of H are present (commonly in technical Ti structures), brittle TiH_2 hydrides are produced, enhancing the propagation of microcracks.

Additionally, a circular crown (rim) appears on the outer edge of the hole, corresponding to a lower energy density, consistent with the Gaussian energy distribution.

The values obtained through numerical simulation are in agreement with the experimental data summarized in Tables 2, 3, validating the developed models and providing possible explanations for the material

5. Conclusions

The study pointed out the performances of single pulse laser machining on materials of significant industrial importance and wide applicability, namely anodized Al 1050 alloy, AISI 304 stainless steel, and technically pure 99.5% Ti, which have low machinability through conventional cutting technologies due to their high strength and surface layer hardness.

Numerical simulations of the ablation process were conducted, and the results obtained from running the computational models were validated by experimental results and by examining the processed surfaces using SEM with 1 nm resolution. The research highlighted complex material removal mechanisms, particularly for anodized Al 1050. The value of this coefficient has an effect at the initial stage of machining, increasing the material removal process.

From the behavior comparison of the AISI 304 and Ti grade 2 at single laser pulse machining, microcracks were observed at the latter material caused by its lack of ductility, and its crystalline structure that presents fewer slip planes. Higher thermal conductivity and lower thermal expansion coefficient also facilitate microcracks emerging. Both materials displayed microcavities, but Ti alloy exbits also spongy surface structure probably due to the phenomenon of fragilization with H, that also enhances the microcracks.

Possible technological solutions to reduce the formation of microcavities include: defocusing, i.e., increasing the laser spot size on the processed surface to decrease energy density, and reducing the energy per pulse by shortening its duration, i.e., using pulses

shorter than 10 ms to minimize vaporization. Using a processing regime similar to ablation can lead to the elimination of this phenomenon, and minimization of the heat-affected zone, This is essential for applications in medicine. This is also significant for micro-and nanotechnologies required in the current stage of development, Industry 4.0.

6. FURTHER RESEARCH

Additional experiments are needed to validate the solutions concerning the adjustment of working parameters, convective force cooling by assisting gas, and improvement of laser focalization.

7. ACKNOWLEDGEMENTS

The single laser pulse machining was achieved by the courtesy of CETAL Magurele management.

8. REFERENCES

1. Marinescu, N.I., Ghiculescu, D., et al., *Technological processes with beams, oscillations and jets*, Vol. 1, Laser Beam Technologies, Printech, Bucharest (2017).
2. Chrisey D.B., Hubler G.K., editors. *Pulsed Laser Deposition of Thin Films,* 1st ed. New York: Wiley, 648 p. (1994).
3. Wang, M., Zhang, T., Yuan, Y., Wang, Z., Liu, Y., & Chen, L. Simulation and Experimental Study of the Single-Pulse Femtosecond Laser Ablation Morphology of GaN Films, *Micromachines*, *16*(1), 85, (2025).
4. Faik Derya Ince, Tuğrul Özel, Laser surface texturing of materials for surface functionalization: A holistic review, *Surface and Coatings Technology*, Volume 498,131818, ISSN 0257-8972, (2025).
5. * * * Laser Texturing, Available at: What Is Industrial Laser Ablation? | Laserax, Accessed at: 16.09.2025.
6. Anugop B, Sithara P. S., Kailasnath M., Sabu T., Dermot B., Nanoparticle production via laser ablation synthesis in solution method and printed electronic application - A brief review, *Results in Engineering*, Volume 16, 100646, ISSN 2590-1230, (2022).
7. Brand, J., Lopez, A.J., Moreno-Madariaga, A. et al. Femtosecond laser ablation for the conservation of Galician granites. *Bull. Eng. Geol. Environ.* 84, 383 (2025).
8. Jingzhen Shao, Xu Liang, Ying Lin, Qihui Shen, Jiacheng Ren, Jinliang Han, Excimer laser marking − A precise patterning technique for material surfaces, *Optics & Laser Technology*, Volume 176, 110974, ISSN 0030-3992, (2024).
9. Hohmann, M., Kühn, D., Ni, D. et al., Relevant parameters for laser surgery of soft tissue, *Scientific Reports* 14, 1263 (2024).
10. Syed Kifayat Hussain Shah, Javed Iqbal, Pervaiz Ahmad, Mayeen Uddin Khandaker, Sirajul Haq, Muhammad Naeem, Laser induced breakdown spectroscopy methods and applications: A comprehensive review, *Radiation Physics and Chemistry*, Volume 170, 108666, ISSN 0969-806X, (2020).
11. Popescu Camelia, Dorcioman, Gabriela, Popescu, A., Laser Ablation Applied for Synthesis of Thin Films: Insights into Laser Deposition Methods, December. In book: Yang, Dongfang, *Applications of Laser Ablation - Thin Film Deposition, Nanomaterial Synthesis and Surface Modification,* InTech (2016).
12. Sallé, Béatrice, Lacour, J.-., Vors, Evelyne, Fichet P., Maurice S., Cremers, D. A., Wiens, R. C., Laser-Induced Breakdown Spectroscopy for Mars surface analysis: capabilities at stand-off distances and detection of chlorine and sulfur elements, *Spectrochimica Acta Part B: Atomic Spectroscopy*, Volume 59, Issue 9, p. 1413-1422, ISSN 0584-8547, (2004).
13. Wu, Z., Lyu, Y., Zhang, Y. et al. Large-scale growth of few-layer two-dimensional black phosphorus. *Nature Materials,* 20, 1203–1209 (2021).
14. * * *, Aluminum 1050, Thyssenkrupp, available at: https://www.thyssenkrupp-materials.co.uk/aluminium-1050, accessed at: 18.09.2025.
15. F.A. Bruera, G.R. Kramer, M.L. Vera, A.E. Ares, Evaluation of surface pretreatment stages of Al 1050 to obtain nanostructured anodic films, *Superlattices and Microstructures*, Volume 130, p. 103-116, ISSN 0749-6036, (2019).
16. * * *, AISI 304 | 1.4301 | BS 304S31 | X5CrNi18-10 | Austenitic stainless steel, Available at: https://www.agst.de/4301?lang=en , Accessed at: 18.09.2025.
17. * * *, Ti Gr2 (Grade 2), SaglaMetal, Available at: https://www.saglammetal.com/en/titanium-alloys/other-alloys/ti-gr2-grade-2-pure-titanium#:~:text=Ti%20Gr2%20(Grade%202%20titanium,iron%2C%20carbon%2C%20and%20nitrogen, accessed at: 18.09.2025
18. * * * Tecnobisa, TRUMPF Laser systems brochure, Available at: https://www.tecnobisa.com, Accessed at: 18.09.2025;
19. * * * TRUMPF, Disk Laser TruDisk, Technical data sheet, Available at: https://www.trumpf.com, Accessed at: 18.09.2025;

20. D'Oliveira, Ana Sofia & Paredes, R.s.C. & Weber, F.P. & Vilar, Rui, Microstructural changes due to laser surface melting of an AISI 304 stainless steel. *Materials Research*, Vol. 4, No. 2, 93-96, (2001).
21. Emelyanenko, K. A., Emelyanenko, A. M., & Boinovich, L. B. Laser Obtained Superhydrophobic State for Stainless Steel Corrosion Protection, a Review. *Coatings*, *13*(1), 194, (2023).
22. Qiuchi Zhu, Wanting Sun, Yongchul Yoo, Xiang Zhang, Nicholas Hunter, Aofei Mao, Nan Li, Xi Huang, Peixun Fan, Xinwei Wang, Bai Cui, Yongfeng Lu, Enhance corrosion resistance of 304 stainless steel using nanosecond pulsed laser surface processing, *Surfaces and Interfaces*, Volume 42, Part B, 103479, ISSN 2468-0230, (2023).
23. Laser Surface Texturing of Stainless Steel − Effect of Pulse Duration on Texture's Morphology and Frictional Response, *Advanced Engineering Materials* 21(3), (2018).
24. Liu, X., Wang, H., & Zhang, Q., Comparative Study of Laser-Induced Microstructural Changes in Titanium and Stainless Steel Alloys, *Journal of Materials Processing Technology*, 310, 117763, (2022).
25. Zhang, Y., Li, Z., & Chen, L., Oxidation and Hydrogen Embrittlement Behavior of Commercially Pure Titanium during High-Temperature Laser Processing, *Corrosion Science*, 215, 111047, (2023).